ChemComm

Accepted Manuscript

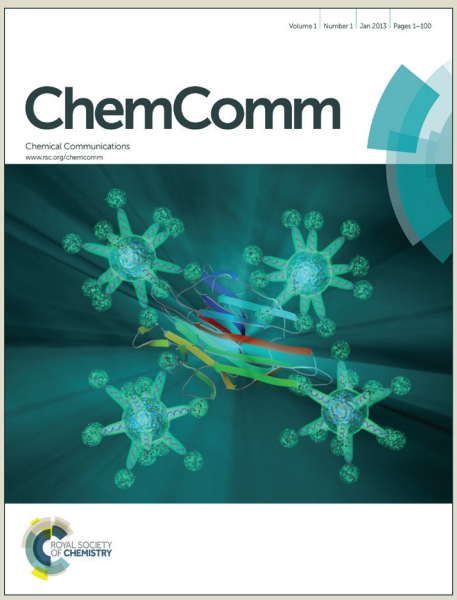

ROYAL SOCIETY OF CHEMISTRY

www.rsc.org/chemcomm

ChemComm

RSCPublishing

COMMUNICATION

Ultrathin carbon layer coated MoO_2 nanoparticles for high-performance near-infrared photothermal cancer therapy†

Cite this: DOI: 10.1039/x0xx00000x

Received 00th January 2012,
Accepted 00th January 2012

DOI: 10.1039/x0xx00000x

www.rsc.org/

Qin Liu,[a] Chunyang Sun,[b] Qun He,[a] Daobin Liu,[a] Adnan Khalil,[a] Ting Xiang,[a] Ziyu Wu,[a] Jun Wang[b] and Li Song*[a]

Carbon layer-coated molybdenum dioxide nanoparticles exhibit strong photo-absorption in the near infrared (NIR) region and pose good photostability. The *in vitro* and *in vivo* experiments reveal that an excellent photothermal ablation induced from the nanoparticle agents under NIR irradiation can kill tumor cells not only at the cellular level but also in living organs.

As one of most promising minimally invasive cancer treatments, light-induced photothermal ablation (PTA) therapy has attracted tremendous attention. PTA employs light absorbing materials to generate heat from light irradiation, which has a large penetration depth and precise spatial control in biological tissues, leading to cancer cells death and tumors destruction.[1]Because the absorption of tissue penetrating light is a prerequisite, only materials with strong near-infrared light absorption are commonly selected as for PTA agents. Among them, nanoscale materials have been extensively studied for PTA application, mainly because that nanostructures can exhibit tunable localized surface plasmon resonance (LSPR) at visible and NIR wavelength region, resulting in enhanced light absorption and scattering.[2] In principle, excitation of LSPR fundamentally relies on the interaction between free charge carriers and light. For examples, both noble metals and metal's nanostructures were found to exhibit strong light-matter interaction because of their high density of free electrons.[3,4] Meanwhile, LSPR has also been observed in heavily-doped metal chalcogenides semiconductor and metal oxide nanocrystals (NCs), which is attributed to the high density of free charge carriers introduced by doping, i.e. copper deficient copper chalcogenides,[5,6] oxygen deficient metal oxides,[7-10] MS_2 (M=Mo/W) nanosheets with mixed 1T and 2H phases,[11,12] Tin-doped indium oxide (ITO)[13] and ZnO doped with group III elements.[14]Recently, LSPR has been reported in graphene and carbon nanotube as collective excitation of 2D mass less Dirac electrons.[15-17]Polypyrrole nanoparticles were used as a promising photothermal agent for *in vivo* cancer therapy.[18]Topological insulator was found to assign Dirac plasmon excitations to Dirac quasi particles of the conducting two-dimensional edge state[19,20]. Surface modification, i.e. coating silica on Pd nanosheets, was employed to significantly improve its photothermal cell-killing efficacy due to the positive charge on the surface [21].

Compared with general heavily-doped semiconductors that need complex and expensive synthesis procedures, a class of conducting metal oxides (CMOs) without any doping also has plasma frequencies due to their intrinsic electronic structure. Furthermore, CMOs can be proposed as promising alternative plasmonic materials to conventional gold materials in the near-infrared range, because the carrier concentration is limited to around 10^{21} cm^{-3}.[22] However, the photothermal application of pure CMOs without any doping are rarely reported so far. Molybdenum dioxide (MoO_2) with a distorted rutile structure is an attractive transition conducting metal oxide because of its metallic electrical resistivity and high chemical stability. [23, 24] However, to the best of our knowledge, MoO_2has not been reported for photothermal cancer treatment. Meanwhile, selective synthesis of oxide-based photothermal agents with low cost and earth-abundance still remains a challenge till now. In this work, we synthesize ultrathin carbon layer-coated MoO_2 hybrid nanoparticles (abbreviated as C/MoO_2) with uniform aggregated diameter of ~120 nm by a facile solvothermal method. Taking advantage of the strong NIR absorbance and the great stability in physiological solutions, the C/MnO_2 nanoparticles with PEGylated exhibit high efficient PTA for cancer cells. We suggest that the following results may trigger intensive future explorations of new hybrid CMOs in cancer therapeutics. This new route will open up the possibility of controllable preparation of hybrid conductive transition metal oxides to significantly extend their potential applications in cancer therapy.

Solvothermal reaction was used to synthesis C/MoO2 nanoparticles in sealed autoclave system (see detail experiment in ESI†). Fig. 1a presents a typical scanning electron microscope (SEM) image taken from as-prepared nanoparticles. It can be seen that numerous nanoparticles with an aggregated diameter of around 100 nm were successfully prepared by solvothermal process. The XRD patterns in Fig. 1b performed on the as-prepared samples reveal that the nanoparticle products can be assigned to monoclinic MoO_2 phase with a distorted rutile structure (JCPDS card No. 76-1807). The low magnification TEM image in Fig. 1c represents that couple of tiny MoO_2 nanoparticles attached each other to form very small aggregation. Fig. 1d shows a typical high-resolution TEM

image taken from the corner of an individual nanoparticle. It can be seen that the surface of individual MoO_2 nanoparticle is tightly coated by thin carbon layers with 1-2 nm thickness, which effectively prevent MoO_2 particles from big aggregation. The estimated 0.34 nm d-spacing is assigned to the interplanar distance between (110) planes of monoclinic MoO_2, which is in good agreement with our XRD results. Dynamic light scattering (DLS) measurement performed on C/MoO_2 aqueous solution is used to calculate the diameter distribution of stable C/MoO_2 particles. The DSL data in Fig. 1e indicate that the main diameters of stable C/MoO_2 particles is approximately 120 nm, no big aggregation was formed even after several months which may be contributed from the outer carbon-coated surface. It can be seen from Raman spectra in Fig. 1f that typical Raman peaks for both MoO_2 and carbon film appear at the frequency range of 100-1800 cm^{-1}, further confirming the hybrid structure of C/MoO2 nanoparticles. FT-IR data that the 1626 cm^{-1} transmission band is assigned to the stretching vibrations of C=C of sp^2 structure also confirm that the existence of carbon (see Figure S1 in ESI†).

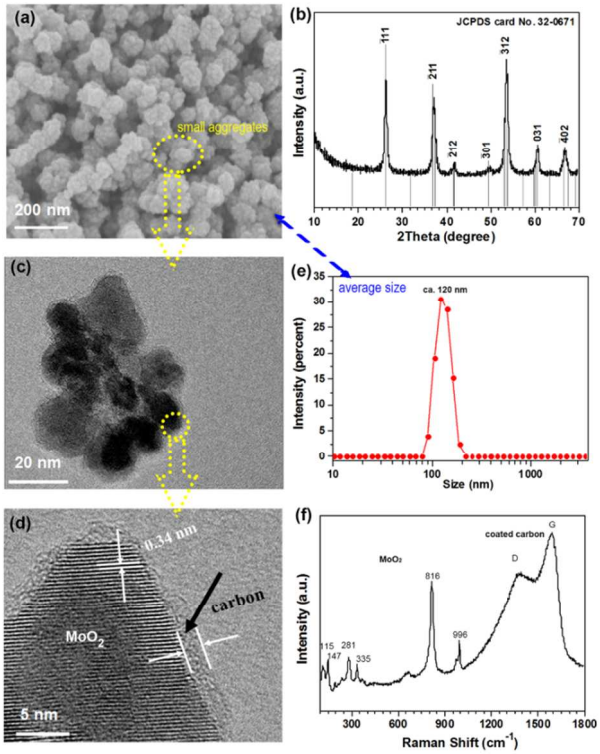

Fig. 1 Typical SEM image (a), XRD patterns (b), low magnification TEM and high-resolution TEM images (c, d), DSL analysis (e) and Raman spectrum of as-prepared carbon-coated MoO_2 hybrid nanoparticles.

The UV-Vis-NIR absorption spectra in Fig. 2a displays strong NIR optical absorption behaviour of C/MoO_2 nanopaticles. The strong light absorption at NIR region motivates us to study light-induced photothermal effect in the C/MoO_2 nanoparticles. The temperature curve in Fig. 2b shows the temperature of an aqueous dispersion containing different nanoparticle's concentrations (0-1 mg ml^{-1}) under the 808 nm laser irradiation with a power of 0.6 W cm^{-2} (a value considered safe for a human skin exposure).[25] It can be clearly seen that there is rapid elevation in temperature for all tested C/MoO_2 solutions, while a negligible change occurs for pure water. A dramatic change in the temperature occurred in the solution containing 1 mg ml^{-1}C/MoO_2 nanoparticles from 22 to 53°C within 5 min under laser irradiation with density of 0.6 W cm^{-2}. For comparison, the temperature curve of pure MoO_2 nanoparticle aqueous solutions with different concentrations were carried out under the same laser irradiation (see Figure S2 in ESI†). The temperature curve shows that 1 mg ml^{-1} pure MoO_2 nanoparticles increase from 22.38 to 50.03°C within 5 min under laser irradiation. However, compared with the intrinsically poor photostability of pure MoO_2 (see Figure S3 in ESI†), Fig. 2c shows the UV-vis-NIR spectra of aqueous C/MoO_2 dispersions before and after laser irradiation at the power density of 0.6 W/cm^2 for 1 h. It is suggested that the hybrid nanoparticles exhibit great photostability without any significant decrease in optical absorbance even after laser exposure for 1 h, in contrast to high cost and poor photostability of widely used gold nanorods. The photothermal effect of C/MoO_2 nanoparticles clearly points out that the nanoparticles can lead to rapid and quick conversion of NIR laser irradiation into heat, which is mainly originated from the MoO_2 nanoparticle due to its localized surface plasmon resonance. Meanwhile, the good photostability of the hybrid are mainly attributed to the ultrathin carbon-coated nanoarchitecture.

Fig. 2 (a) UV-vis-NIR spectra taken from C/MoO_2 nanoparticles powder. (b) The temperature increase of the aqueous C/MoO_2dispersions with different

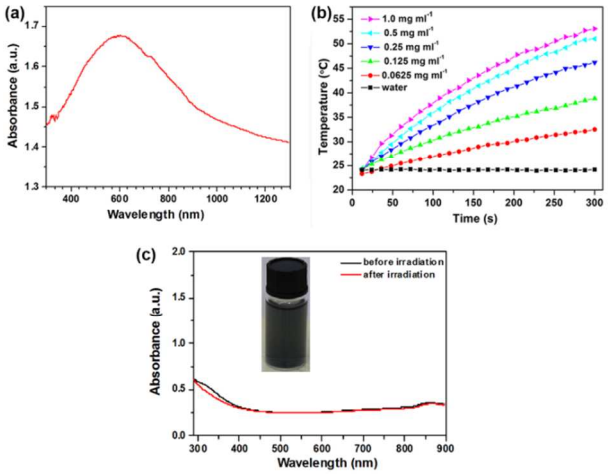

concentrations vs. time under NIR laser irradiation at the power density of 0.6 W cm^{-2}. (c) UV-vis-NIR spectra of aqueous C/MoO_2 dispersions before and after laser irradiation at the power density of 0.6 W/cm^2 for 1 h. The inset image is a typical photography of C/MoO_2 aqueous solutions.

It is well known that the ideal photothermal coupling agents should be biocompatible. Typically, PEGylated process is considered as a common treatment for improving the biocompatibility of various nanomaterials. Thus, we have used thiol functionalized polyethylene glycol (SH-PEG) to modify the surface of C/MoO_2 nanoparticles (see detail in ESI†). The successful modification of PEG-SH and corresponding content were demonstrated by FT-IR and TGA measurements (see Figure S1 and S4 in ESI†). In order to evaluate the cytotoxicity of PEGylated C/MoO_2 nanoparticles, MDA-MB-231 cells (human mammary epithelial cell line), HepG2 cells (human hepatocellular carcinoma cell line) and BxPC-3 cells (human pancreas carcinoma cell line) cells were cultured with nanoparticles solution, and the cytotoxicity was studied by a standard methyl thiazolyltetrazolium (MTT) assay after 24 h. The estimated cellular viability in Fig. 3a is larger than 90% after 24 h even at the highest concentration of 400 μg mL^{-1}. No significant difference in the cell proliferation can be observed among the three cell lines, indicating the good biocompatibility of the hybrid nanoparticles to cells. All these observations suggest that the aqueous dispersion containing the nanoparticles with concentration <400 μg mL^{-1} can be considered as low or negligible cytotoxic for biological applications.

In vitro photothermal ablation capacity of the nanoparticles on MDA-MB-231 cells was evaluated via MTT assay. In experimental processes, we incubated MDA-MB-231 cells, cancer cells with the nanoparticles at the concentration of 60 μg ml^{-1} for 6 h, then irradiated them with an 808 nm NIR laser at different power densities (see detail experiment in ESI†). The cell viability in Fig. 3b is larger than 95% of total cells without laser irradiation, while it decreases as a function of the irradiated laser power density. The proliferation rate of MDA-MB-231 cells is only ~25% of the control after laser irradiation at the power density of 0.8 W cm^{-2}. Meanwhile, we have measured the cell viability at the fixed laser density of 0.6 W cm^{-2} with different nanoparticles concentrations. It is observed from Fig. 3c that the cell viability significantly decreases with the increasing concentration of nanoparticles. The cell viability is ~80% at the concentration of 12.5 μg ml^{-1} and further decreased to ~20% at the concentration of 100 μg ml^{-1}. In contrast to this, the control groups are not affected under laser irradiation even for long time. This result points out that the cancer cells are substantially unaffected by 808 nm laser irradiation with power density<0.6 W cm^{-2}, and the ablation could be mainly attributed to the photothermal effect induced by the nanoparticles.

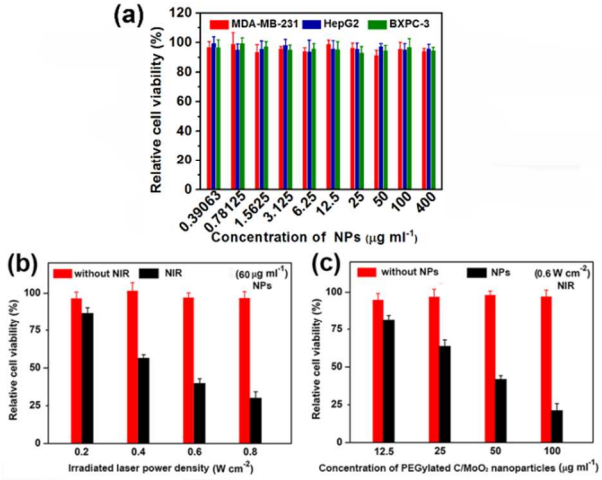

Fig. 3 (a) The cell viability of MDA-MB-231, HepG2 and BxPC-3 cells after incubation with different concentration of PEGylated C/MoO_2 nanoparticles for 24 h.(b) MDA-MB-231 cells viability cultured with the nanoparticles at 60 μg mL^{-1} with or without laser irradiation for 10 min. (c) cell viability of MDA-MB-231 cultured with different concentration of the nanoparticles and then irradiated with the same laser power 0.6 W cm^{-2} for 10min.

To further demonstrate the photothermal potential, *in vivo* NIR irradiation experiments using BALB/c nude mice bearing the MDA-MB-231 tumors were performed on PEGylatedC/MoO_2 nanoparticles. In our experiments, 40 μL of nanoparticles and PBS were injected intratumorally, followed by irradiation using an 808 nm NIR laser at the power density of 0.6 W cm^{-2} (see detail experiment in ESI†). Fig. 4a shows the thermal images of the interested regions at different time interval as recorded by an infrared camera. We analyzed the average surface temperature of tumor sites throughout the photothermal therapy by IR Flash Software (Infrared Cameras. Inc). Fig. 4b exhibits that the average temperature of tumors in the PBS group without NIR irradiation remains constant at ~26 °C. Similar behavior is also observed for the non-irradiated nanoparticle group (NPs). For the control experiment of NIR group, only 1-2 °C change is detected when the NIR radiation hits tumors due to the laser heating. In contrast to the control experiments, the temperature for the nanoparticles group exposed to NIR laser irradiation (NPs+NIR) dramatically increased to 47 °C (an increase of ~21 °C) within 4 min and subsequently remained constant around 47 °C for next 6 min. It has been previously reported that a tumor could be completely destroyed under a high temperature increase (> 15 °C) in ~5 min.[26-28] An overall increase in temperature to 20 °C suggests that power density and concentrations used in our work are accurate for the proposed tumor treatment. Besides, we found that the temperature increases only in a small area around the tumor site while other organs are not affected, thanks to the spatial control of NIR laser irradiation.

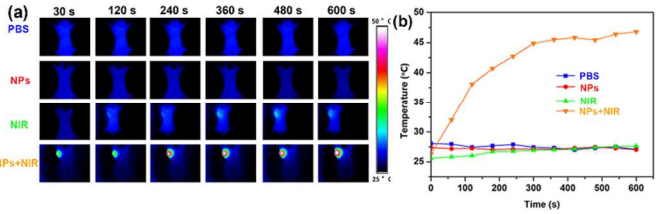

Fig. 4 (a) Thermal infrared images of tumor-bearing mice treated with PEGylated C/MoO_2 nanoparticles and an 808 nm NIR laser irradiation of 0.6 W cm^{-2} at different time intervals. As control experiments, other mice groups received only PBS, nanoparticles injection or laser irradiation. (b) The plots of the temperature in tumor sites vs. the irradiation time.

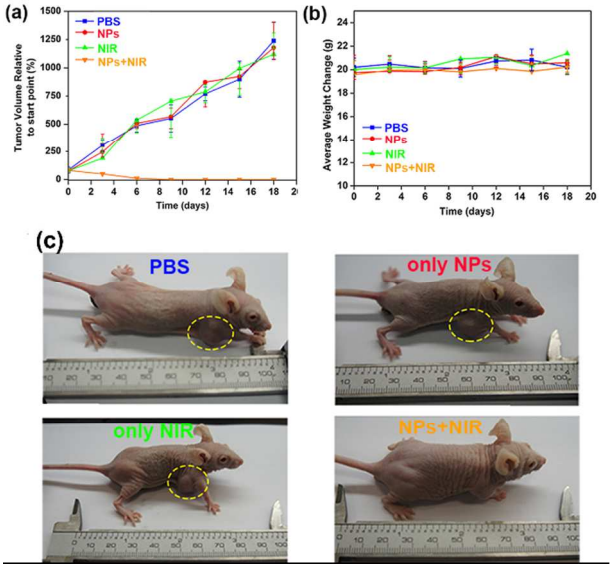

Fig. 5 (a) The growth of the tumor after different treatments on MDA-MB-231 tumors-bearing BALB/c nude mice (n = 5).The mice groups that only received PBS, nanoparticles injection and laser irradiation are marked as PBS,NPs and NIR. The group with PEGylated C/MoO_2 nanoparticles and 808 nm NIR laser irradiation of 0.6 W cm^{-2} is marked as NPs+NIR. (b) The body weight of the mice during the different photothermal therapy. (c) Representative photos of mice taken after various treatments within 7 days.

Furthermore, *in vivo* tumor ablation treatment was also carried out to deeply understand the PTA potential of the nanoparticles. Mice bearing MDA-MB-231 tumors were randomly divided into four groups (5 mice each). When the average tumor size achieved to about 100 mm^3, the nanoparticles were injected intratumorally. NPs+NIR group with only one dose (concentration and power density were the same as in the imaging experiment) while other groups received only PBS or NIR irradiation. The tumor sizes were monitored by a capillary routinely after every three days and calculated with the following formula: 0.5´length´$width^2$ (see detail experiment in ESI†). Fig. 5a shows that the tumor growth was not inhibited in the control groups (mice that received only NIR irradiation, injection of PBS or nanoparticle). It is observed that after 18 days the dimension of the tumor in the control groups is about 15 times greater as compared to the initial tumor size. On the contrary, all of the tumors disappeared in the NPs+NIR group after 7 days of NPs+NIR treatment due to the photothermal ablation induced from the nanoparticles. It is worth noting that no tumor recurrence can be

observed after the whole treatment process. In order to further evaluate the influence of various treatments, we monitored the body weight of mice during the photothermal experimental process. Fig. 5b shows that the weight of mice is relatively stable and remains at its normal value in all groups. Meanwhile, the autopsy performed on the treated mice indicated no abnormalities in liver, lungs and other organs, suggesting a good biocompatibility and a low toxicity effect of hybrid MoO_2-based PTA treatment. Fig. 5c show representative photos of mice after various treatments within 7 days. In contrast to the big-size tumors in control groups, the MDA-MB-231 tumors in mice for NPs+NIR group clearly disappeared after 7 days treatment. Moreover, for further clarification of mechanism of photothermal therapy, we collected tumors for the H&E stain after two days of NIR irradiation treatment. Fig. S6 shows that significant cell damage can be clearly observed in the NPs group undergoing NIR laser irradiation in contrast with the control groups. These observations indicate that the elimination of tumors originates from the excellent photothermal ablation of C/MoO_2 nanoparticles, not due to the material's toxicity itself.

Conclusions

In summary, we demonstrated a simple and versatile approach to synthesize ultrathin carbon layer-coated molybdenum dioxide nanoparticles with uniform size of 120 nm by a solvothermal process. Our characterizations showed that the hybrid C/MoO_2 nanoparticles exhibited strong plasmonic-enhanced photo absorption at near-infrared region with good photostability. The *in vitro* and *in vivo* experiments revealed that the cancer cells incubated with nanoparticles (1 mg ml^{-1}) can be efficiently killed after 808 nm NIR laser irradiation with powder density of 0.6 W cm^{-2} for 5 min. More intriguingly, *in vivo* tumor ablation performed on mice bearing MDA-MB-231 tumors revealed that excellent treatment efficacy can be obtained by intratumoral injection of the nanoparticles and NIR laser irradiation, without noticing significant side effects after treatment. The subsequent characterizations indicated that the photothermal effect of hybrid C/MoO_2 nanoparticles was mainly originated from the localized surface plasmon resonance in MoO_2 nanoparticles, and the good photostability and biocompatibility of the hybrid were attributed to the ultrathin carbon coating nanoarchitecture. The presented results suggest that the new C/MoO_2 nanoparticles can be used as promising NIR photothermal agents to induce local higher temperature for killing tumor cells not only at the cellular level but also in living organs.

Financial supports come from 973 program (2012CB825800, 2014CB848900), NSF (U1232131, 11375198) and the Fundamental Research Funds for the Central Universities (WK2310000035). L.S. thanks the recruitment program of global experts and the CAS Hundred Talent Program of China

Notes and references

[a]National Synchrotron Radiation Laboratory, University of Science and Technology of China, Hefei, Anhui 230029, China

[b]Hefei National Laboratory for Physical Science at the Microscale, School of Life Sciences, University of Science and Technology of China, Hefei, Anhui 230027, China.

E-mail: song2012@ustc.edu.cn

†Electronic Supplementary Information (ESI) available: Experimental details and data. See DOI: 10.1039/c000000x/

1 X. Huang, I. H. El-Sayed, W. Qian, M. A. El-Sayed, *J. Am. Chem. Soc.,* 2006, **128,** 2115.

2 P. D. Howes, S. Rana and M. M. Stevens, *Chem. Soc. Rev.,* 2014,**43,** 3835.

3 H. J. Chen, L. Shao, Q. Li and J. F. Wang, *Chem. Soc. Rev.,*2013, **42,** 2679.

4 S. Jelveh and D. B. Chithrani, *Cancers,* 2011, **3,** 1081.

5 J. M. Luther, P. K. Jain, T. Ewers and A. P. Alivisatos, *Nat. Mater.,* 2011, **10,** 361.

6 W. H. Li, R. Zamani, P. R. Gil, B. Pelaz, M. Ibáñez, D. Cadavid, A. Shavel, R. A. Alvarez-Puebla, W. J. Parak, J. Arbiol, and A. Cabot, *J. Am. Chem. Soc.,* 2013, **135,** 7098.

7 C. M. Hessel, V. P. Pattani, M. Rasch, M. G. Panthani, B. Koo, J. W. Tunnell and B. A. Korgel, *Nano Lett.,* 2011, **11,** 2560.

8 C. S. Guo, S. Yin, H. J. Yu, S. Q. Liu, Q. Dong, T. Goto, Z. W. Zhang, Y. P. Li and T. Sato, *Nanoscale,* 2013, **5,** 6469

9 G. Song, J. Shen, F. Jiang, R. Hu, W. Li, L. An, R. Zou, Z. Chen, Z. Qin and J. Hu, *ACS Applied Materials & Interfaces,* 2014, **6,** 3915.

10 B. Li, Y. Zhang, R. Zou, Q. Wang, B. Zhang, L. An, F. Yin, Y. Hua, J. Hu, *Dalton Transactions,* 2014, **43,** 6244.

11 L. Cheng , J. J. Liu , X. Gu, H. Gong, X. Z. Shi, T. Liu, C. Wang, X. Y. Wang, G. Liu, H. Y. Xing, W. B. Bu, B. Q. Sun and Z. Liu, *Adv. Mater.,* 2013, **26,**1886.

12 W. Y. Yin, L. Yan, J. Yu, G. Tian, L. J. Zhou, X. P. Zheng , X. Zhang, Y. Yong, J. Li, Z. J. Gu and Y. L. Zhao. *ACS Nano,* 2014, **8,** 6922.

13 A. Llordes, G. Garcia, J. Gazquez and D. J. Milliron, *Nature,* 2013, **500,** 323.

14 E. D. Gaspera, M. Bersani, M. Cittadini, M. Guglielmi,D. Pagani, R. Noriega, S. Mehra, A. Salleo and A. Martucci, *J. Am. Chem. Soc.,* 2013, **135,** 3439.

15 L. Ju, B. S. Geng, J. Horng, C. Girit, M. Martin, Z. Hao, H. A. Bechtel, X. G Liang, A. Zettl, Y. R. Shen and F. Wang, *Nature Nanotech,* 2011,**6,**630.

16 T. Isoniemi, A. Johansson, T. K. Hakala, M. Rinkiö, P. Törmä, J. J. Toppari1 and H. Kunttu, *Appl. Phys. Lett.,* 2011, **99,** 031105.

17 J. T. Robinson, S. M. Tabakman, Y. Y. Liang, H. L. Wang, H. S. Casalongue, D. Vinh and H. J. Dai, *J. Am. Chem. Soc.,* 2011, **133,** 6825.

18 M. Chen, X. L. Fang, S. H. Tang and N. F. Zheng, *Chem.Comm.,*2012,**48**, 8934.

19 P. D. Pietro, M. Ortolani, O. Limaj, A. D. Gaspare, V. Giliberti, F. Giorgianni, M. Brahlek, N. Bansal, N. Koirala, S. Oh, P. Calvani and S. Lupi, *Nature Nanotech,* 2013, **8,**556.

20 J. Li, F. Jiang, B. Yang, X. R. Song, Y. Liu, H. H. Yang, D. R. Cao, W. R. Shi and G. N. Chen, *Sci. Rep.,* 2013, **3,** 1.

21 S. H. Tang, X. Q. Huang and N. F. Zheng, *Chem. Comm.,* 2011,**47,** 3948.

22 G. Naik, J. Kim and A. Boltasseva. *Opt. Mater. Express,* 2011, **1**, 1090.

23 Magneli, A. Andersson, G. *Acta Chem. Scand.,* 1955, **9,** 1378.

24 D. B. Rogers, R. D. Shannon, A. W. Sleight and J. L. Gillson, *Inorg.Chem.,* 1969, **8,** 841.

25 B. P. Timko, Tal Dvir and D. S. Kohane, *Adv. Mater.,* 2010*,* **22,** 4925.

26 C. L. Peng,Y. H. Shih, P. C. Lee, T. M. H. Hsieh, T. Y. Luo, M. J. Shieh, *ACS Nano,*2011, **7,** 5594.

27 J. L. Zhang, W. J,X. Q. Wang, J.C. Wang, X. Zhang, Q. Zhang, *Molecular Pharmaceutics,*2010,**7,** 1159.

28 J. Yang, H. Y. Wang, W. J. Yi, Y. H. Gong, X. Zhou, R. X. Zhuo, X. Z. Zhang, *Adv. Healthcare Mater.,*2013, **2,** 481.

